Icarus 322 (2019) 121–134

Contents lists available at ScienceDirect

Icarus

journal homepage: www.elsevier.com/locate/icarus

On the principal building blocks of Mars and Earth

Christian Liebske[a,*], Amir Khan[b]

[a] Institute of Geochemistry and Petrology, ETH Zürich, Switzerland
[b] Institute of Geophysics, ETH Zürich, Switzerland

ARTICLE INFO

Keywords:
Mars
Earth
Oxygen isotopes
Nucleosynthetic isotopes
Chondrites
Bulk composition

ABSTRACT

The terrestrial planets are believed to have been formed from primitive material sampling a broad region of the inner solar system. Several meteoritic mixing models attempting to reconcile isotopic characteristics of Mars and Earth have been proposed, but, because of the inherent non-uniqueness of these solutions, additional independent observations are required to resolve the question of the primary building blocks of the terrestrial planets. Here, we consider existing isotopic measurements of $\Delta'^{17}O$, $\epsilon^{48}Ca$, $\epsilon^{50}Ti$, $\epsilon^{54}Cr$, $\epsilon^{62}Ni$, and $\epsilon^{84}Sr$ for primitive chondrites and differentiated achondrites and mix these stochastically to reproduce the isotopic signatures of Mars and Earth. For both planets we observe $\sim 10^5$ unique mixing solutions out of 10^8 random meteoritic mixtures, which are categorised into distinct clusters of mixtures using principal component analysis. The large number of solutions implies that isotopic data alone are insufficient to resolve the building blocks of the terrestrial planets. To further discriminate between isotopically valid mixtures, each mixture is converted into a core and mantle component via mass balance for which geophysical properties are computed and compared to observations. For Mars, the geophysical parameters include mean density, mean moment of inertia, and tidal response, whereas for Earth upper mantle Mg/(Mg + Fe) ratio and core size are employed. The results show that Mars requires an oxidised, FeO-rich differentiated object next to chondritic material as main building blocks. In contrast, Earth's origin remains enigmatic. From a redox perspective, it appears inescapable that enstatite chondrite-like matter constitutes a dominant proportion of the building blocks from which Earth is made. The apparent need for compositionally distinct building blocks for Mars and Earth suggests that dissimilar planetesimal reservoirs were maintained in the inner Solar System during accretion.

1. Introduction

All Solar System planets are thought to have accreted from material that was present in, or condensed from the solar nebula (Taylor, 2001). This primitive material is present today in the form of chondrites, which provides a window into the earliest stages of planet formation. To deduce any compositional relationships between known meteorites and terrestrial planets, identification of the material from which the planets accreted and differentiated into core, mantle, and crust is required. The question of the nature of "the building blocks" of the terrestrial planets has, however, remained elusive because of the perceived difficulty in constructing planets from known meteoritic material (Drake and Righter, 2002; Righter et al., 2006). Early models of the bulk compositions of Mars and Earth (e.g., Dreibus and Wänke, 1984; Taylor, 1980) suggested a genetic relation to carbonaceous chondrites, particularly CI, which represent a class of undifferentiated meteorites whose relative element abundances closely resemble that of the solar photosphere (Anders and Grevesse, 1989). For example, in the widely-used model of Dreibus and Wänke (1984), Mars was proposed to have accreted from two components, one third of oxidised CI-like material and two thirds of highly reduced material, possibly enstatite chondrite-like matter. This interpretation was based on major, minor, and trace element concentrations in Martian meteorites and the assumption that certain element ratios (e.g., Mg/Si) are identical to CI.

For the Earth it has been argued that carbonaceous chondrites provide a better match to Earth's volatile depletion trend than any other known type of chondrite (Allègre et al., 2001; Palme and O'Neill, 2003). Palme and O'Neill (2003) also suggested that Earth's Mg/Si ratio is best matched by carbonaceous chondrites, assuming that a proportion of Si is sequestered into the core. However, these interpretations are far from unique given the increasing amount of high-precision stable isotope measurements of a number of elements in primitive, differentiated, and planetary material which has become available over the last decade (e.g. Schönbächler et al., 2005; Trinquier et al., 2007; Dauphas et al., 2014; Qin and Carlson, 2016). The importance of considering these measured isotopic anomalies stems from the observation of unique

* Corresponding author.
E-mail address: christian.liebske@erdw.ethz.ch (C. Liebske).

https://doi.org/10.1016/j.icarus.2019.01.014
Received 25 July 2018; Received in revised form 10 January 2019; Accepted 14 January 2019
Available online 20 January 2019
0019-1035/

Table 1
Chemical compositions used in this study. Chondritic end-members are from Wasson and Kallemeyn (1988), recalculated as core and mantle components using redox information reported by Jarosewich (1990) and Burbine and O'Brien (2004). Values are normalised to 100 wt.%. Compositions for APB and EPB are based on Ashcroft and Wood (2015), Jurewicz et al. (1991), and Steenstra et al. (2017) (see main text for details). Sr (in ppm) values for APB and EPB are estimates.

	CI	CM	CO	CV	EH	EL	H	L	LL	APB	EPB
Oxides and carbon											
SiO_2	27.7	30.0	35.8	35.5	36.7	41.7	36.5	40.1	41.5	28.1	37.6
TiO_2	0.09	0.12	0.13	0.16	0.08	0.10	0.10	0.11	0.11	0.10	0.50
Al_2O_3	2.0	2.4	2.7	3.3	1.6	2.1	2.2	2.3	2.3	2.7	3.0
Cr_2O_3	0.48	0.48	0.53	0.53	0.49	0.47	0.54	0.57	0.56	0.40	0.20
FeO	19.9	23.3	20.4	26.7	0	0	10.4	14.3	16.8	24.9	12.0
MnO	0.30	0.24	0.21	0.19	0.30	0.22	0.30	0.34	0.35	0.20	0.10
Sr (ppm)	7.9	10.1	12.7	15.3	7.2	8.2	10	11.1	11.1	10	10
MgO	19.8	21.1	23.8	24.0	18.8	24.7	23.5	25.0	26.0	20.2	26.0
CaO	1.6	1.9	2.2	2.7	1.3	1.5	1.8	1.9	1.9	2.1	2.5
Na_2O	0.81	0.60	0.55	0.44	0.98	0.83	0.87	0.96	0.97	0.033	0.090
K_2O	0.10	0.05	0.04	0.04	0.10	0.09	0.09	0.10	0.10	0.003	0.008
P_2O_5	0.29	0.22	0.24	0.23	0.49	0.28	0.25	0.22	0.20	0.19	0.084
H_2O	11.6	8.9	0.5	0.2	0	0	0	0	0	0	0
C	3.0	1.9	0.2	0.4	0.4	0.3	0.1	0.1	0.2	0	0
Metal and sulfide											
Fe	0	0.1	4.4	0.2	22.3	18.3	16.2	7.0	2.4	10.6	9.1
FeS	11.0	7.2	6.8	4.0	13.7	7.8	5.6	5.8	5.6	9.1	7.8
Ni	1.3	1.3	1.4	1.3	1.9	1.4	1.6	1.2	1.0	1.3	1.1
Co	0.06	0.06	0.07	0.06	0.09	0.07	0.08	0.06	0.05	0	0
Si	0	0	0	0	0.7	0.2	0	0	0	0	0

1) H_2O and C are assigned to the silicate components, but expected to be volatile and lost to space.
2) Sulfur is expressed as FeS and C as elemental carbon, which is a simplification especially in the case of CI chondrites.
3) FeO is assumed to be the only iron oxide species.
4) Ni and Co are exclusively assigned as core components, which neglects partitioning between core and mantle.

isotope signatures among the various meteorite groups (Trinquier et al., 2007; Warren, 2011) that may contain clues to the origin of the planets.

For Mars, models consisting of a variety of mixtures of different meteoritic classes have been put forward based on the isotopic composition of the Martian meteorites (Lodders and Fegley, 1997; Sanloup et al., 1999; Mohapatra and Murty, 2003; Burbine and O'Brien, 2004; Tang and Dauphas, 2014; Fitoussi et al., 2016; Brasser et al., 2017). However, adjustments to mantle and core mass are required for some current Mars models to match present-day geophysical observations (Khan et al., 2018). Specifically, Khan et al. (2018) considered the bulk chemical Martian models of Dreibus and Wänke (1985), Lodders and Fegley (1997), Sanloup et al. (1999), and Taylor (2013) and found that each model required adjustments to e.g., bulk Fe/Si ratio, core sulfur content and/or core size to match current geophysical constraints. This implies that several bulk Mars models are unable to self-consistently explain major element chemistry and geophysical properties simultaneously. Likewise, models that rely on Earth's stable isotopic composition (Javoy, 1995; Lodders, 2000; Burbine and O'Brien, 2004; Javoy et al., 2010; Warren, 2011; Dauphas et al., 2014; Dauphas, 2017) have been used to argue in favour of either enstatite chondrites or enstatite chondrite-like material given the isotopic similarity.

Thus, while there have been several attempts to determine the terrestrial planetary building blocks from isotopic compositions of chondritic material (Lodders and Fegley, 1997; Sanloup et al., 1999; Mohapatra and Murty, 2003; Burbine and O'Brien, 2004; Fitoussi and Bourdon, 2012; Tang and Dauphas, 2014; Dauphas et al., 2014; Dauphas, 2017; Brasser et al., 2017) and mixtures of chondritic and achondritic (differentiated) objects (Fitoussi et al., 2016), a systematic high-resolution investigation that probes the entire isotopic and geophysical solution space simultaneously is lacking. This is partly because of the intractably large number of possible meteorite mixtures that need to be investigated (Burbine and O'Brien, 2004) and partly because geophysical data have been given less weight in the context of building terrestrial planets. In spite of this, the question if any of the previous mixing solutions are unique remains to be understood.

To address these outstanding issues, we build upon the statistical mixing models of Burbine and O'Brien (2004) and Fitoussi et al. (2016) and extend their methods to reconcile geochemical signatures, geophysical properties, and redox characteristics of Mars and Earth. We obtain a large isotopic solution space and employ principal component analysis to determine several distinct mixing clusters. Complementary geophysical and redox analysis limits the number of favourable mixtures among the clusters. While the emphasis here is on Mars, the method is applied in a simplified form to Earth with the ultimate goal of inferring the extent to which planetary building blocks varied compositionally within the inner solar system.

2. Methods

2.1. The geochemical model

The geochemical model calculates isotopic signatures and bulk compositions for random mixtures of potential building blocks of the terrestrial planets. We include carbonaceous (CI, CM, CO, CV), ordinary (H, L, LL), and enstatite chondrites (EH, EL), and two types of differentiated achondrites, angrites, and eucrites, in our model. For all of these meteorite types we consider isotopic values for $\Delta'^{17}O$, and nucleosynthetic anomalies of $\epsilon^{48}Ca$, $\epsilon^{50}Ti$, $\epsilon^{54}Cr$, $\epsilon^{62}Ni$, and $\epsilon^{84}Sr$. Ca, Ti, and Sr are lithophile elements and are thus unaffected by core-forming processes in comparison to the moderately siderophile elements Cr and Ni, for which no evidence for isotopic fractionation between core and mantle reservoirs exists (Bonnand et al., 2016; Cook et al., 2007). A working assumption of mixing models including lithophile and moderately siderophile elements (e.g., Dauphas et al., 2014; Fitoussi et al., 2016) (to which we shall also adhere), is that the nature of the accreted material does not change with time, as assumed in homogeneous accretion. Otherwise siderophile elements tend to record later stages of accretion as discussed by Dauphas (2017).

All chemical compositions and isotope data that are used in this study are summarised in Tables 1 and 2. The bulk chemical data for the undifferentiated chondrites are from Wasson and Kallemeyn (1988), recalculated as "silicate" and "core"- fraction using the redox information of Burbine and O'Brien (2004) and Jarosewich (1990). The isotopic data for all objects are taken from the compilation of Burkhardt

Table 2
Isotopic values used in this study. All values are taken from a recent compilation of Burkhardt et al. (2017), except ϵ^{54}Cr for Earth, for which a weighted average of data from Mougel et al. (2018) are used.

	Δ'^{17}O	±	ϵ^{48}Ca	±	ϵ^{50}Ti	±	ϵ^{54}Cr	±	ϵ^{62}Ni	±	ϵ^{84}Sr	±
CI	0.07	0.28	2.05	0.20	1.85	0.12	1.56	0.06	0.20	0.14	0.40	0.10
CM	−2.52	0.46	3.4	1.00	3.01	0.10	1.02	0.08	0.10	0.03	0.40	0.09
CO	−4.21	0.68	3.87	0.56	3.77	0.50	0.77	0.33	0.11	0.03	0.41	0.21
CV	−3.99	0.33	3.92	0.50	3.65	0.34	0.87	0.07	0.11	0.03	0.63	0.10
EH	−0.09	0.12	−0.32	0.56	−0.14	0.07	0.04	0.08	0.03	0.03	−0.21	0.12
EL	−0.04	0.08	−0.38	0.26	−0.24	0.21	0.04	0.07	−0.03	0.07	−0.21	0.20
H	0.67	0.10	−0.24	0.30	−0.64	0.17	−0.36	0.08	−0.06	0.03	−0.13	0.10
L	0.97	0.09	−1.17	0.68	−0.63	0.08	−0.4	0.10	−0.04	0.03	−0.11	0.21
LL	1.11	0.11	−0.15	0.39	−0.66	0.14	−0.42	0.07	−0.07	0.03	−0.43	0.10
APB	−0.08	0.06	−1.27	0.15	−1.18	0.08	−0.43	0.15	0.01	0.05	0.00	0.10
EPB	−0.24	0.06	−1.33	0.37	−1.23	0.05	−0.67	0.09	0.03	0.12	0.01	0.10
Mars	0.25	0.06	−0.11	0.72	−0.49	0.23	−0.18	0.05	0.04	0.03	−0.25	0.15
Earth	−0.05	0.06	0	0.1	0	0.1	0.12	0.05	0	0.05	−0.19	0.16

1) ϵ^{48}Ca of CM is estimated based on interpolation of carbonaceous chondrites in ϵ^{48}Ca vs ϵ^{54}Cr space.
2) ϵ^{84}Sr of EL is estimated to be identical to ϵ^{84}Sr of EH, but the uncertainty is increased by 50%.

et al. (2017), updated with data for ϵ^{54}Cr from Mougel et al. (2018) (Table 2). The achondrites (angrites and eucrites) represent a class of differentiated objects, which implies that the bulk composition of their parent bodies (angrite parent body, APB and the eucrite parent body, EPB) differ in bulk chemistry from the known meteoritic compositions. We assume that the modelled isotopic systems do not fractionate in magmatic or core-forming events and that the measured isotopic values for angrites and eucrites (see below) are representative of their parent bodies. For the eucrite parent body (EPB), we use the chemical composition proposed by Ashcroft and Wood (2015) with a core mass of 18%, which is consistent with measurements of the Dawn mission to 4 Vesta (Russell et al., 2012), considered to be the EPB. There are only a few studies for the bulk estimate of the angrite parent body, but it is usually assumed to be relatively oxidised, i.e. with a high silicate FeO content. Jurewicz et al. (1993) have argued that liquids similar to angrite compositions can form by partial melting of a volatile depleted CV-like bulk chemistry. This implies a relatively simplistic basalt generation mode, but in the absence of more sophisticated estimates, the composition of Jurewicz et al. (1991) with volatile (Na_2O, K_2O) depletion by a factor of 10, will be used (see Table 1). We note that although the volatile depletion might be higher than assumed here, this has no effect on the calculated geophysical properties, due to the low general abundance of these components. We assume a core mass of 21%, consistent with a recent estimate based on the observed siderophile element depletion in angrites (Steenstra et al., 2017). The actual core composition for both, APB and EPB, is poorly constrained. We assume that the cores consist exclusively of Fe, Ni, and S and use the solar system relative abundances (Anders and Grevesse, 1989) for these elements to calculate the core compositions as reported in Table 1. The consequences of the uncertainty surrounding the bulk compositions of ABP and EPB will be discussed below.

Random mixtures of chondrites or chondrites plus achondrites are generated using a Monte-Carlo method. The mass fractions x for N meteorite classes in a given mixture are determined from the following steps:

- A meteorite class $j \in [1,\ldots,N]$ is chosen at random and its mass fraction x is determined from a randomly generated integer α:

$$x_j = \alpha_j/100, \quad \alpha_j \in [0;\ 100]$$

- This procedure is repeated:

$$x_k = \alpha_k/100, \quad \alpha_k \in [0;\ 100-\alpha_j], \quad k \in [1,\ldots,N]\setminus\{j\}$$
$$\vdots$$
$$x_m = \alpha_m/100,\ \alpha_m \in [0;\ 100-\alpha_j-\alpha_k\ldots-\alpha_l], \quad m \in [1,\ldots,N]\setminus\{j,\ k,\ldots,\ l\},$$

until $\sum_{i=1} x_i = 1$.

- In mixtures where N–1 meteorite classes have been allocated, but $\sum_{i=1}^{N-1} x_i < 1$, the last chosen class will be assigned the maximum allowable mass fraction to ensure closure, i.e., $\sum_{i=1}^{N} x_i = 1$.

The chemical composition of the resulting mixtures is then calculated from mass balance, such that the concentration c of a chemical component m in the mixture is the sum over all weight fractions x_i multiplied by the concentrations of m in that component, c_i^m,

$$c_{\mathrm{Mix}}^m = \sum_{i=1} x_i \cdot c_i^m. \tag{1}$$

If an isotope ratio of m involving the mass of interest τ is used, the ϵ (or Δ in the case of oxygen) value in the final mixture is calculated as

$$\epsilon^\tau m_{\mathrm{Mix}} = \frac{\sum_{i=1} x_i \cdot c_i^m \cdot \epsilon^\tau m_i}{c_{\mathrm{Mix}}^m}, \tag{2}$$

which weights the isotopic signals based on the actual abundances of m within each meteorite class. Some of the isotopic data reported in Table 2 show considerable variability expressed as large 2-sigma errors. To account for this variation we calculate the resulting isotopic signature for each random mixture 250 times, by imposing a Gaussian distribution for each isotope value, such that approximately 95% of the drawn, random isotope values fall within the average and its reported uncertainty. If all isotopic anomalies fall simultaneously within the range of uncertainties for either Mars or Earth, as reported in Table 2, the mixture is considered a match.

All matching mixtures are then filtered for duplicates and analysed using principal component analysis (PCA). PCA is a standard technique for the analysis of multivariate solution spaces and particularly useful in the present context to reveal systematics of isotopically valid mixtures between the different meteorite groups. PCA transforms the N original variables of the dataset (here the weight fractions of meteorite groups) into a set of N linearly uncorrelated, principal but "abstract" components. PCA maximises the variance of the data with respect to the first principal component, and then maximises the remaining variance across the second component, and so forth. As a result, data can generally be described with a number of principal components $\ll N$ without significant loss of information. The general methodology and procedure to generate PCA-derived figures as displayed below is described in detail elsewhere (Liebske, 2015).

2.2. The redox model

The metal and sulfide fractions of the resulting mixtures are assumed to form the core and all other chemical components are assigned

to the silicate proportion, i.e. mantle and crust. We assume that sulfide is the only S-bearing species and that it is entirely incorporated into the core (see Section 2.3). These mass balanced chemical compositions may not be in equilibrium with each other and undergo redox reactions, which alter the initial distribution of core-forming material and mainly FeO in the silicate proportion. Water and carbon are expected to be the main species to interact with iron or iron oxide. Previous studies have used specific H_2O, C, Fe and FeO-involving reactions, applied in a defined order, to derive the final redox state of meteoritic mixtures (Lodders and Fegley, 1997; Sanloup et al., 1999; Burbine and O'Brien, 2004). However, that such an approach is unlikely to predict to final redox state correctly without a more rigorous thermodynamic approach. Instead, we consider all mixtures in their initial redox state and calculate the effect for two end-member scenarios, which define the maximum possible extent of oxidation and reduction by water and carbon, respectively:

$$Fe_{core} + H_2O = FeO_{mantle} + H_2 \quad (3)$$

and

$$2FeO_{mantle} + C = 2Fe_{core} + CO_2 \quad (4)$$

In both cases we assume the reaction to proceed completely to the righthand side and that gaseous products (H_2, CO_2) do not further react, i.e, that they are either lost to space or remain largely isolated from metal-silicate reactions in an early atmosphere. We emphasise that both scenarios are just mass balance considerations and realistic redox changes are somewhere in-between, also due to reactions between the two redox species. Furthermore, both reactions represent simplifications as we ignore the presence of Fe_2O_3, which could reduce both the oxidation and reduction capacity of H_2O and C, respectively, by additional reactions. The first reaction implies oxidation of core material and will result in a decrease of core mass and a simultaneous increase of the mantle FeO content, whereas the second reaction has the opposite effect.

The only explicit redox reaction that we apply for the simulations on Mars and prior to geophysical modelling, is that any Si dissolved in the core fractions of EH and EL chondrites is subsequently oxidised by reduction of mantle FeO according to:

$$Si_{core} + 2FeO_{mantle} = SiO_{2,mantle} + 2Fe_{core} \quad (5)$$

This reaction reduces the core system to a pseudo-binary (Fe,Ni)-S and is consistent with a redox state of the primitive Martian mantle around the iron-wuestite buffer (Wadhwa, 2001) at which the partitioning of Si into metal is negligible (Mann et al., 2009). For Earth this reaction may proceed from right to left for a given mixture to explain a high proportion of Si metal as light element in the core (Javoy, 1995).

2.3. The geophysical model

To convert the geochemical compositions derived from mass balance (Section 2.1) into geophysically testable models, we make use of phase equilibrium computations to compute radial models of geophysical properties (e.g., P- and S-wave speed and density). From the latter, geophysical responses (mean mass and moment of inertia and tidal response) can be predicted for direct comparison to observations. The methodology follows our geophysical inverse study (Khan et al., 2018), to which the reader is referred for more details.

Martian compositions are explored in the NaO_2-CaO-FeO-MgO-Al_2O_3-SiO_2 model chemical system. This chemical model accounts > 98% of terrestrial mantles (Taylor, 1980; Dreibus and Wänke, 1984). Here, Martian mineralogy and physical properties are assumed to be governed by thermodynamic equilibrium and computed for a given model pressure, temperature, and bulk composition along self-consistent adiabats by Gibbs free-energy minimisation (Connolly, 2009) using the thermodynamic formulation and parameters described in Stixrude and Lithgow-Bertelloni (2005) and Stixrude and Lithgow-Bertelloni (2005).

For the core, we also follow our earlier study (Khan et al., 2018) and assume the core to be a binary mixture of Fe-S, which is entirely liquid, well-mixed, and convecting. For this purpose, we rely on the parameterisation of Rivoldini et al. (2011). Thermoelastic properties for the core are computed using equations-of-state for liquid iron and liquid iron-sulfur alloys. This is based on the observation in support of a liquid Martian core from orbiting spacecraft measurements of the tidal response of Mars (Yoder et al., 2003; Konopliv et al., 2016; Genova et al., 2016). This suggests low liquidus temperatures consistent with Fe-FeS eutectic-like compositions (e.g. Stewart et al., 2007) and therefore, a sulfur-rich core. Additional evidence in support of core S enrichment comes from the observed depletion of chalcophile elements of the Martian meteorites (Dreibus and Wänke, 1984; McSween and McLennan, 2014). The case for sulfur as light-element core-component is discussed further by Rivoldini et al. (2011). Note that while core Fe and S content are parameters, these are not determined independently of the mantle composition, but are related to the FeO content of the latter through the exchange redox reactions mentioned earlier. For example, an increase of one mole in mantle FeO is balanced by a decrease of one mole Fe in core mass.

To compute radial profiles of geophysical properties from the surface to the centre, we consider a spherically symmetric model of Mars, which has been divided into a number of discrete layers. The thermodynamic calculations are commenced at the surface and properties are computed at depth intervals of 25 km in the mantle and 100 km in the core, providing adequate resolution. Crust and lithospheric temperature conditions are computed by a linear thermal gradient. The sublithospheric mantle is assumed uniform and the mantle adiabat is defined by the entropy of the lithology at the temperature at the base of the lithosphere, which defines the location of the intersection of the conductive lithospheric geotherm and mantle adiabat. The crust is probably more complex lithologically, not equilibrated, and porous. We consider porosity by decreasing the seismic properties of the crust. For the crust, we consider the average crustal composition of Taylor and McLennan (2009) and assume a mass fraction of 0.05, corresponding to a crustal thickness of 50 km. The required parameters are taken from Khan et al. (2018) and are summarised in Table 5. The mantle pressure profile is obtained by integrating the vertical load from the surface pressure boundary condition. Mean mass and moment of inertia are computed by simple integration of the density profile, whereas the tidal response (amplitude and phase) at the main period of Phobos (5.55 h) is

Table 3
Summary of geophysical data for Mars, including uncertainties. Calculation of the elastic tidal response (k_2) refers to the main tidal period of Phobos (5.55 h). The values for the mean moment of inertia and mass have been updated (Rivoldini et al., 2011) using the latest determination of GM for Mars with G = 6.67408(31) × 10^{11} $m^3/kg{\cdot}s^2$ (Konopliv et al. (2016)).

Observation	Symbol	Value (± uncertainty)	Source
Mean density	ρ_M	3.9350 ± 0.0004 g/cm^3	Esposito et al. (1992)
Mean moment of inertia	I/MR^2	0.3638 ± 0.0001	Konopliv et al. (2016)
Love number	k_2	0.169 ± 0.006	Konopliv et al. (2016)
Mean radius	R	3389.5 km	Seidelmann et al. (2002)
Mean mass	M	$6.417 \cdot 10^{23} \pm 2.981 \cdot 10^{19}$ kg	Konopliv et al. (2016)

Table 4
Summary of average cluster maxima from principal component analysis for all simulations on Mars and Earth. *n* refers to the number of similar mixtures at the cluster maximum (see Figs. 2a, 5a, 7a).

Cluster	n	CI	CM	CO	CV	EH	EL	H	L	LL	APB	EPB
Mars (chondrites)												
EH + H	81	0.9	0.9	0.7	0.5	44.1	0.5	50.7	0.9	0.8	-	-
EH + L	86	0.6	1	0.9	0.7	51	0.5	0.1	44.4	0.8	-	-
EH + LL	165	0.7	0.7	0.7	0.5	60.7	2.2	0.4	1.4	32.7	-	-
EL + H	48	0.5	0.4	0.1	0.4	0.7	56.1	38.2	1.6	2	-	-
EL + L	115	0.7	0.6	0.4	0.4	1	62.5	0.4	31.5	2.5	-	-
EL + LL	179	0.3	0.9	1.1	0.8	1.9	58.2	1	3.5	32.3	-	-
Mars												
EH + H	300	0.7	0.7	0.5	0.4	42.6	0.7	49.2	0.2	0.8	2.8	1.5
$(EH + L)_1$	31	1.3	0.3	0.3	0.5	53.7	0.4	0.7	37.9	0.8	2.8	1.4
$(EH + L)_2$	35	0.4	0.2	0.1	0.1	72.9	0.4	0.3	20.2	0.4	2.7	2.3
EH + LL	52	0.4	0.3	0.1	0.2	73.6	0.5	2.6	0.7	16.3	2.7	2.7
EL + H	147	0.4	0.2	0.3	0.1	1.6	50.8	37.4	0.8	1.9	4.2	2.2
EL + L	50	0.3	0.5	0.5	0.3	0.3	63	0.5	31.9	0.5	1	1.3
EL + LL	85	0.2	0.5	0.4	0.3	0.3	65.8	0.4	0.1	29.3	1.4	1.3
cC + L + EPB	200	2.3	7.6	3.3	1.9	0.1	0.2	0.4	68.8	0.6	1.1	13.8
cC + LL + EPB	280	1.5	6.9	4.5	3	0.1	0.2	0.5	0.4	64.7	1.9	16.5
cC + LL + APB	210	2.9	6.2	2.8	2.1	0.7	0.5	1.9	0.4	51.8	21.6	9.2
Earth												
EH	1065	1.3	1.2	0.9	0.8	88.5	0	2	1.8	1.6	1.5	0.5
EL	1166	1.1	1.6	1	1.1	0	89.7	1.5	1.1	1.5	0.9	0.5
cC + L + APB	164	15.7	9.4	3.2	2.2	0.2	0.1	5.3	30.1	9.8	18.3	5.7

Table 5
Summary of model parameters used for computing geophysical properties. NCFMAS refers to the oxides NaO_2-CaO-FeO-MgO-Al_2O_3-SiO_2. Prior range is taken from Khan et al. (2018). In the inversions, parameters X_{mantle}, X_S, and R_{core} are not independently variable, but subject to the core-mantle mass exchange reaction (Section 2.1).

Parameter	Description	Value	Prior range
$1 - \phi_0$	Surface porosity	0.35	0.35–0.5
d_{moho} (km)	Crustal thickness	50	50–80
T_{surf} (°C)	Surface temperature	−100	Fixed
T_{lit} (°C)	Lithospheric temperature	1350	1350–1460
d_{lit} (km)	Lithospheric thickness	200	200–400
X_{crust}(*wt.%*)	Crustal composition (NCFMAS)	Taylor and McLennan (2009)	Fixed
X_{mantle} (wt.%)	Mantle composition (NCFMAS)	Mass balance	Variable
X_S (wt%)	Core composition (S content)	Mass balance	Variable
R_{core} (km)	Core radius	Mass balance	Variable

computed using a viscoelastic tidal code (Roberts and Nimmo, 2008).

Finally, because of uncertainties in the Martian temperature profile, the effect of the assumed parameters on the computed geophysical data was tested by running the entire model suite of compositions at T_0, $T_0 + 75$ K, and T_0-75 K, which corresponds to the mean thermal profile and its variance determined by Khan et al. (2018).

2.4. Geophysical inversion

Here we briefly describe our method for inverting the Martian geophysical observations for core and mantle masses (the results are described in Section 3.1). The inverse problem can formally be written as $\mathbf{d} = g(\mathbf{m})$, where $\mathbf{d}$ is a data vector consisting of observations and g embodies the forward operator that enables us to compute data from a given model $\mathbf{m}$. The inverse problem is solved using a Bayesian approach (Mosegaard and Tarantola, 1995) that combines prior information on model parameters with information from data and physical models

$$\sigma(m) = kf(m)\mathcal{L}(m), \tag{6}$$

where k is a normalisation constant, $f(\mathbf{m})$ is the prior model parameter probability distribution, $\mathcal{L}(m)$ is the likelihood function, and $\sigma(\mathbf{m})$ is the posterior model parameter distribution. Prior information (Table 5) represents information on model parameters obtained independently of data and the likelihood function measures the misfit between observed and predicted data. Assuming that data noise is Gaussian distributed and that observational uncertainties and calculation errors are independent among the data, the likelihood function can be written as

$$\mathcal{L}(m) \propto \prod_i \exp\left(-\frac{|d^i_{obs} - d^i_{cal}(\mathbf{m})|^2}{2\sigma_i^2}\right) \tag{7}$$

where i is either ρ_M, I/MR^2, or k_2; d_{obs} and $d_{cal}(\mathbf{m})$ denote observed and calculated data, respectively, and σ data uncertainty.

To sample the geophysical model space, we employ the Metropolis algorithm; an importance sampling algorithm that ensures that models that fit data well, and are simultaneously consistent with prior information, are sampled more frequently. In practice, the algorithm operates by performing a "guided" random walk in the model space. At each iteration a new model is sampled according to the prior distribution whose misfit is tested against the data through the likelihood function. Depending on whether datafit has improved or not, the proposed model is either accepted or rejected based on a specific acceptance criterion (Mosegaard and Tarantola, 1995). The inversion scheme was run for 10 million iterations and every 100th model was retained to ensure near-independent samples. Model parameters and prior information are summarised in Table 5. We should note that while all the parameters are determined in the inversion, here we concentrate on the parameters of main relevance, e.g., mantle FeO, MgO, and SiO_2 content, mantle and core mass fractions, and core composition. The other tabulated parameters have nonetheless been checked for consistency and convergence.

3. Results and discussion

Three sets of model simulations are performed of which two are dedicated to Mars and one to Earth. In each model simulation, $2.5 \cdot 10^{10}$ isotopic signatures for $\Delta'^{17}O$, $\epsilon^{48}Ca$, $\epsilon^{50}Ti$, $\epsilon^{54}Cr$, $\epsilon^{62}Ni$, and $\epsilon^{84}Sr$ are generated from 10^8 meteoritic mixtures (Section 2.1). In the first simulation, only mixtures of undifferentiated chondrites (CI, CO, CM, CV, H, L, LL, EL, and EH) are considered, whereas in the second Martian and third terrestrial run, the mixtures are extended to include differentiated

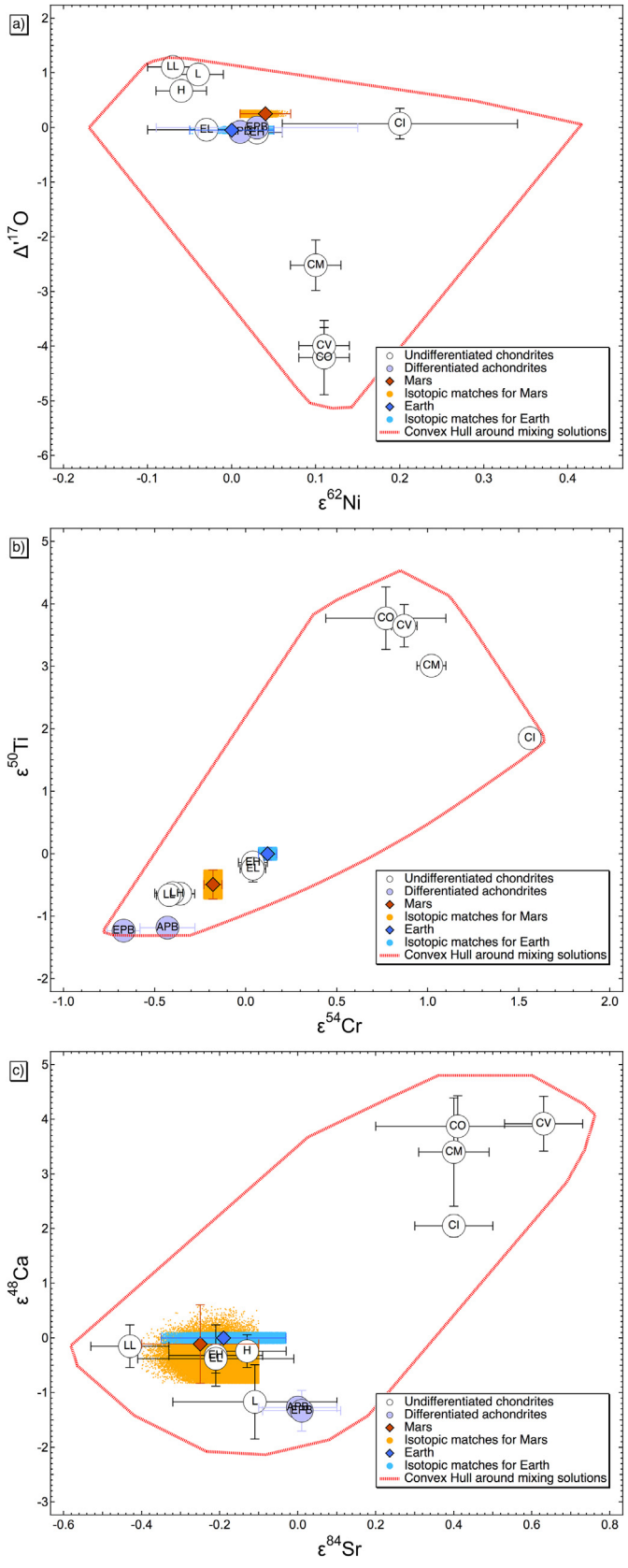

Fig. 1. Isotope variations among meteoritic, terrestrial, and Martian samples. Meteoritic material includes undifferentiated chondrites (CI, CO, CM, CV, H, L, LL, EL, EH) and achondrites (differentiated objects): angrites (APB) and eucrites (EPB). Stable isotope anomalies considered here include: a) $\Delta'^{17}O$ vs $\epsilon^{62}Ni$, b) $\epsilon^{50}Ti$ vs $\epsilon^{54}Cr$, and c) $\epsilon^{48}Ca$ vs $\epsilon^{84}Sr$. Blue and orange regions indicate the isotopic mixtures of chondrites and achondrites, respectively, that reproduce the isotopic anomalies of Mars and Earth within observational error. The entire range of isotopic solutions obtained from mass-balancing random meteoritic mixtures of meteoritic material is indicated by dashed red lines (convex hulls). Isotope anomaly data are summarised in Table 2.

achondrites in the form of angrites and eucrites and compositional estimates for their parent bodies (Ashcroft and Wood, 2015; Jurewicz et al., 1991), as described above. Variations in isotopic values for chondrites, achrondrites, Mars, and Earth are shown in Fig. 1 and display relations between nucleosynthetic isotope systems. The total solution range from mass balancing random weight fractions of meteoritic end-members is indicated by convex hulls for the pairs of isotopes. Any simulated meteoritic mixtures for either Mars or Earth that, within error, simultaneously reproduce the ranges for all isotopes is considered an isotopic match.

3.1. Results for Mars

In the first Martian simulation, where only chondritic mixtures are considered, matches from 102,050 unique mixtures (out of 10^8) are found to produce isotopic matches, resulting in a "match rate" of ~0.1%. The range of weight fractions of the different meteoritic classes in matching solutions is displayed as a histogram in the appendix (Fig. A.8a), which shows that the majority of mixtures contain larger fractions of either EH or H chondrites. While informing, such histograms generally lack information on which combinations of meteorites produce successful isotopic matches. Fig. 2a shows the results from principal components analysis (PCA) of the 102,050 unique solutions. The plot represents a bivariate histogram of the data projected onto first and second principal components, which together account for 85% of the total variance of the dataset. The inset in Fig. 2a shows that typically 4–6 different meteorite groups contribute to the isotopic matches. The different clusters represent high abundances of mixtures for which the indicated meteoritic groups show relatively constant mass fractions, while others are highly variable. For each cluster, the maximum, i.e. the bin pair with the highest number of mixtures, is determined and the average is reported in Table 4 as indication of the weight fractions of meteorite groups that result in isotopic matches. Additionally, the cluster mixtures, together with results to be described in the following section, are shown in a ternary diagram representing the main meteorite classes enstatite-, ordinary, and carbonaceous chondrites (Fig. 3). The bivariate histogram further allows mixing relations between the different clusters to be explored, for example, the near-horizontal trend among the clusters "EL + LL" and "EH + LL" can be interpreted as a continuous exchange between EL and EH, while LL remains almost constant. Similarly, along the vertical direction, substitution of different ordinary chondrite groups (H, L, LL) mixed with either EH or EL can be observed. A few solutions exist that are clearly identifiable as "end-members" in the histogram (top-center), which contain mostly H with up to 10 wt.% carbonaceous chondrites (cC = CI + CM + CO + CV). This also marks the maximum amount of carbonaceous material in a chondrite-only mixture with which it is possible to generate an isotopic match for Mars.

The bulk chemistry for each isotopically matching mixture is calculated from mass balance and is divided into a "core" and "mantle" component (Section 2.1). These compositions are subsequently converted to geophysical properties (e.g., seismic P- and S-wave speeds and density) using Gibbs free energy minimisation for the silicate mantle mineralogy and a parameterised equation-of-state approach for the core, from which bulk geophysical data in the form of mean density (ρ_M), mean moment of inertia (I/MR^2), and elastic tidal response (k_2) are computed (Table 3). The results are shown in Fig. 2b. The figure clearly suggests that none of the isotopically valid chondritic mixtures

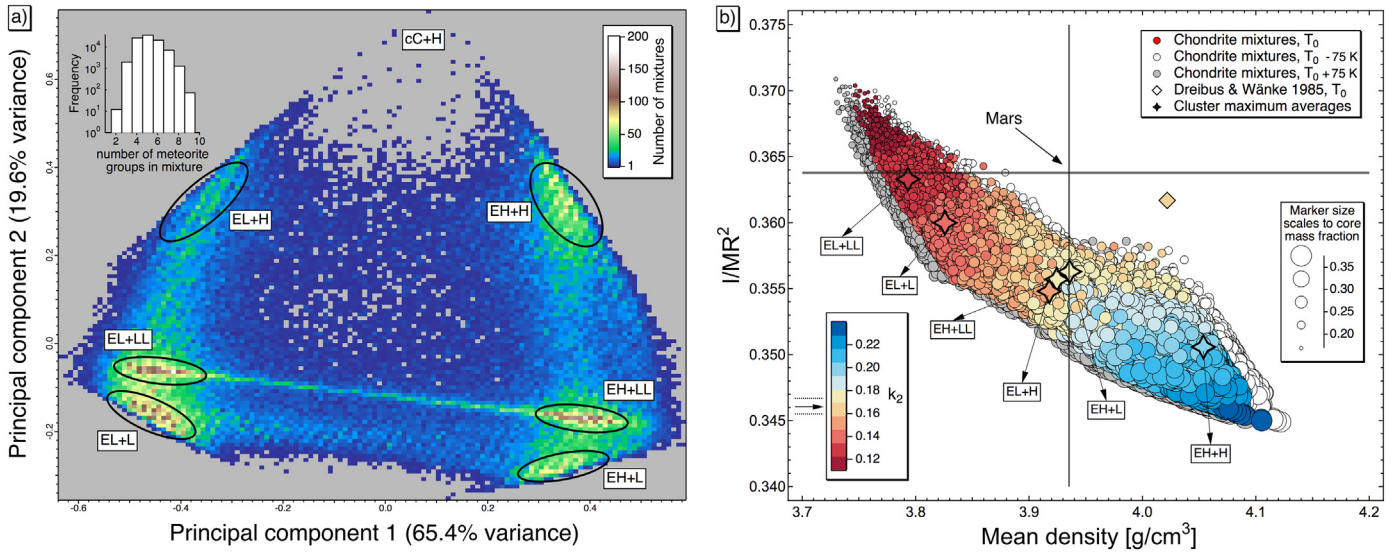

Fig. 2. Results for Mars when considered as a mixture of chondrites only. a) Principal component analysis (PCA) in the form of a density plot of the first two principal components. PCA indicates several clusters of solutions (outlined in black) that are able to match the observed isotopic variation in martian meteorites. The histogram in the inset shows the distribution in number of meteorite groups that contribute to matching solutions. b) Predicted Martian geophysical properties for each of the isotopic solutions: mean moment of inertia (I/MR^2), mean density (ρ_M), and elastic tidal response (k_2) for different thermal conditions. Observed values for I/MR^2, ρ_M, and k_2 are indicated by horizontal and vertical lines and arrows, respectively, and widths show observational uncertainty (see Table 3). The location of the average compositions of the clusters shown in a) are indicated by stars, whereas the yellow diamond indicates the geophysical response of the widely-used bulk Mars composition of Dreibus and Wänke (1984) at the reference thermal condition T_0 (see Fig. A.9). Based on the location of the solutions, the plot shows that purely chondritic mixtures, while matching isotopic anomalies, are unable to simultaneously fit all geophysical observations.

in their original redox states are capable of simultaneously "fitting" all geophysical properties. In particular, I/MR^2, matching for ρ_M and k_2, is significantly lower than current observations for Mars. Note, that employing different areotherms (Fig. A.9) only has a small influence on calculated properties (see grey and white circles in Fig. 2b). Since I/MR^2 is sensitive to the mass distribution within the planet, this implies discrepancies in modelled core and mantle masses relative to Mars. The widely-used bulk Mars compositional model of Dreibus and Wänke (1984) (diamond-shaped symbols in Fig. 2b) also suffers this deficit but changes to core mass fraction and sulfur content can resolve this (Khan et al., 2018).

Based on this observation, three average cluster compositions with similar mean densities compared to Mars (see Fig. 2b, Table 6) are tested further to assess whether these can be optimised to fit the geophysical observations by varying relative core and mantle masses. Compared to the inversion procedure -performed by Khan et al. (2018), we consider the mixtures as isochemical. This implies that core-mantle exchange occurs by a change in redox state from metallic iron (core) to ferrous (mantle), or vice versa, through reactions with the redox partners H_2O or C (Section 2.2). Inversion results are summarised in Table 6 and are reported in terms of characteristic compositional parameters before and after inversion. The results show that geophysical properties can only be matched by decreasing core mass by several wt. % (increases I/MR^2) and implies, from a redox perspective, that chondritic mixtures are too reduced to be consistent with Mars.

Fig. 4 shows the maximum possible redox changes for isotopically matching solutions for Mars sorted by H_2O content. CI chondrite-rich mixtures provide the highest redox change potential because these contain the highest concentrations of both H_2O and C. For example, complete Fe oxidation by water may cause a maximum FeO increase of 4.5 wt. % relative to the initial state calculated from mass balance with a simultaneous change of core mass of −3.5 wt. % (solid lines). For the same mixture, the opposite effect of carbon can cause a maximum increase of 4.4 wt. % core mass coupled with −5.6 wt. % decrease in mantle FeO (dashed lines). Note, that for most mixtures, carbon is more abundant than H_2O, which implies that such compositions may evolve

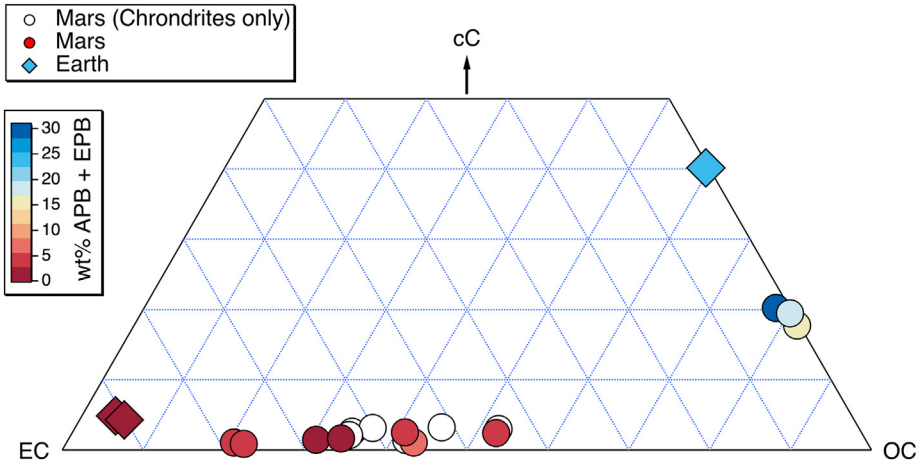

Fig. 3. Cropped ternary diagram (as weight fractions) summarising the average cluster maxima (Table 4) for isotopically valid mixtures for all simulations on Mars and Earth. Only the main meteorite classes, enstatite-, ordinary-, and carbonaceous chondrites are represented here (EC = EH + EL, OC = H + L + LL and cC = CI + CV + CM + CH). Data including APB + EPB (see below) as fourth component are projected from a tetrahedral representation. Circle- and diamond-shaped symbols represent mixtures that can isotopically reproduce the signatures of Mars and Earth, respectively.

Table 6
Model composition obtained from geophysical inversion. For a core-mantle mass exchange (Section 2.1) only two of three clusters can be optimised to fit all current geophysical constraints on Mars (Table 3) ("after inversion"). Core Fe content (x_{Fe}) and mantle mass fraction (X_{mantle}) are obtained from $X_{Fe} = 1\text{-}X_S$ and $X_{mantle} = 1\text{-}X_{core}$, respectively. Visual inspection of inverted model parameter distributions showed these to be Gaussian distributed as a result of which inverted compositions ("after inversion") quoted below refer to the mean of the sampled probability distributions. The last reported digits in parentheses indicate uncertainty (equivalent of ± standard deviation of the probability distributions). "No convergence" identifies the model that could not be made to match the geophysical observations. Note that the present inversions are capable of producing a model (EH + L) with a mantle FeO content as low as 13.5 wt.% (Mg# ~ 0.8), that is consistent with a proposed low-FeO mantle models (Borg and Draper, 2003; Agee and Draper, 2004).

Cluster	CaO (wt.%)	FeO (wt.%)	MgO (wt.%)	Al_2O_3 (wt.%)	SiO_2 (wt.%)	Na_2O (wt.%)	H_2O (wt.%)	C (wt.%)	Mg#	X_S	X_{core}	Comment
EH + LL	2.2	6.3	30.7	3.2	56.2	1.5	0.21	0.5	0.90	0.13	0.29	no convergence
EH + L	2.2	8.0	30.5	3.2	54.6	1.4	0.23	0.41	0.87	0.13	0.28	before inversion
	2.1(0.5)	16.0(5)	27.9(2)	2.8(0.5)	49.9(2)	1.3(1)			0.76	0.164(4)	0.22(1)	after inversion
EL + H	2.2	6.1	32.9	3.4	54.1	1.2	0.13	0.32	0.91	0.1	0.26	before inversion
	2.1(1)	13.5(5)	30.5(3)	3.1(0.5)	50.0(1)	1.1(1)			0.80	0.123(2)	0.21(1)	after inversion

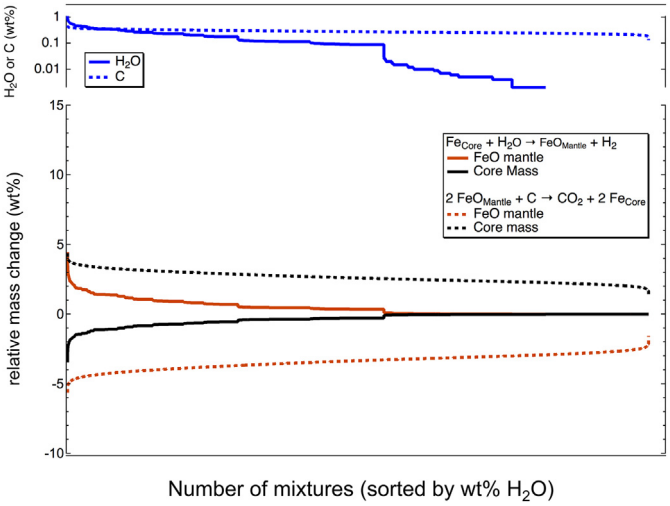

Fig. 4. Maximum possible change in core mass and mantle FeO content caused by redox reactions with either H_2O or carbon. Zero refers to the initial redox state calculated by mass balance. The horizontal axis represents all isotopically valid mixtures (n = 102,050) for Mars accreted from chondrites-only and is sorted after H_2O content. Both reactions shown in the annotation are idealised and unlikely to proceed entirely to the right-hand side. The relative changes in core mass and mantle FeO concentration should therefore be considered as upper limits. The reaction involving carbon assumes sufficient amounts of FeO in the mantle, which in case of reduced EH-rich mixtures, may not always be the case.

towards a more reduced state, i.e., to a core mass that is larger than the initially modelled state. Returning to the inversion results, of the three cluster averages, only the clusters "EH + L" and "EL + H" are capable of matching all geophysical observations. For both of these clusters a change in core mass of ~5–6 wt. % is required, which cannot be achieved with the limited concentrations of H_2O present as oxidant (see Table 6, Fig. 4), which suggests that no isochemical mixture of chondrites is a viable representation of Mars.

In a next step, we simulate Mars by including differentiated objects in the form of the angrite and eucrite parent bodies (APB and EPB) in the chondrite mixtures. Out of 10^8 mixtures, we obtain matches for 185,257 unique combinations (match rate ~0.2%) with an APB or EPB mass fraction of at least 1%. Thus, these mixing solutions are different from the ones discussed in the previous section. The results from this simulation are shown in Fig. 5. PCA indicates additional clusters, mostly dominated by 2–3 meteorite groups including APB or EPB, that are able to match Mars' isotopic composition (see also Table 4, Fig. 3). The existence of the additional solution clusters can be discerned from Fig. 1b (ϵ^{50}Ti vs. ϵ^{54}Cr), where strongly positive signatures of carbonaceous chondrites can be compensated for by the more negative values of APB or EPB in order to match Mars' isotopic composition. The predicted geophysical properties (Fig. 5b) are, relative to purely chondritic mixtures (white circles), considerably extended in the geophysical data space towards larger I/MR^2 values. This is a direct consequence of considering the differentiated objects, since these are assumed to be relatively oxidised and are therefore capable of compensating for the more reduced nature of the chondritic mixtures as discussed above. This observation is also supported by Fig. 6 which shows bulk compositional parameters such as Mg/Si ratio, Mg# (MgO/(MgO + FeO) in moles), and core mass fraction for isotopic matches of chondrites-only and chondrites including APB and EPB. Compared to a mixture consisting of chondrites only, the compositional range in Mg#'s for mixtures including APB and EPB is significantly extended to lower values and lower core mass fractions. Thus, an important conclusion to be drawn from these models is that building Mars requires a relatively oxidised object, such as the APB, in addition to chondritic material. We should note, however, that the bulk chemical compositions of APB and EPB are subject to uncertainty and, as a consequence, the solutions presented in Fig. 5 are only valid for the explicit bulk APB and EPB compositions reported in Table 1. For these particular compositions, matches with < 10% of cC, ~30% of EH, ~40% of LL, and ~20% APB fulfil all isotopic and geophysical constraints.

3.1.1. Comparison with previous isotope models

Several studies have attempted to determine the chemical composition of bulk Mars based on isotopic data and the known primitive undifferentiated meteorites. Lodders and Fegley (1997) and Sanloup et al. (1999) used oxygen isotopes as constraint, while Mohapatra and Murty (2003) also considered nitrogen isotopes. These studies presented explicit mixing and mass balance solutions, supported by simple geophysical considerations to reproduce mean density and the known moment of inertia of Mars at the time (0.365–0.366). Except for the solution presented by Lodders and Fegley (1997), the other previously suggested mixtures are found to be part of our solution space but are inconsistent with current geophysical observations.

In view of the observed difficulty of making planets based on chondritic compositions only, Fitoussi et al. (2016) considered, as a novel approach, to admix differentiated components (e.g., APB and EPB). While their mixing method is statistical and therefore shares similarities with our approach, there are nonetheless differences. For example, Fitoussi et al. (2016) limit the number of allowed meteorite groups to 2–4 in their mixtures and perform a likelihood calculation to minimise isotopic mismatches with the goal of obtaining a set of preferred mixtures. Their best-fit solution for Mars consists of 55% APB, 36% H, and 9% CI, which, when converted into mantle and core components (based on their "Bulk composition of Mars", cf. their Table 2), results in a core size of ~3–4 wt. %. This value presumes that all reported oxygen is bound to silicate with the simplifying assumptions that FeO is the only Fe-bearing species (cf. Section 2.2) and that there are no significant remnants of H_2O or other oxygen-bearing volatile components. Although the core-mantle ratio of their proposed

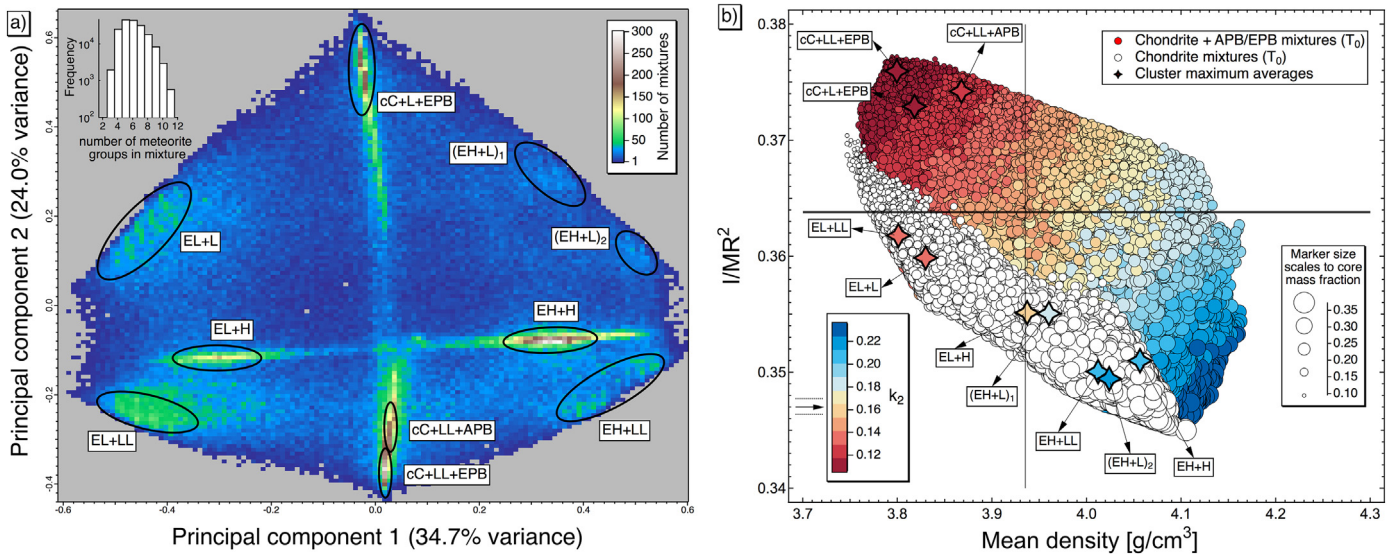

Fig. 5. Results for Mars when considered as a mixture of chondrites and achondrites (differentiated objects): angrites (APB) and eucrites (EPB). a) The principal component analysis density plot shows additional clusters compared to the purely chondritic mixtures (cf. Fig. 2a). b) The geophysical solution space (I/MR^2, ρ_M, and k_2), is significantly extended relative to the chondrite-only case (white circles) and mixtures that match all observations for Mars can be identified (see main text for details).

bulk composition appears to be somewhat low, the authors note that iron and oxygen are subject to uncertainty because of the unknown APB core size. The particular mixture derived by Fitoussi et al. (2016) is not included in the present set of solutions but a very similar one that consists of 55% APB, 35% H, and 10% CI is found. Due to different assumptions surrounding the APB composition, we obtain a resulting core mass of approximately 21 wt. %, although the geophysical properties for this particular mixture (I/MR^2 = 0.362, ρ_M = 4.157, k_2 = 0.194) remain incompatible with current observations.

Fitoussi et al. (2016) have further argued that their APB-rich mixture provides a good match to lithophile elements ratios, such as Na/Sm or K/Th, which are assumed to be insensitive to magmatic events. This assumption is a useful first-order approximation for primitive mantle melting, but not generally true for all stages of magmatic differentiation, particulary those involving fluids (see e.g. Taylor et al., 2007). However, purely chondritic mixtures result in high Na/Sm and K/Th ratios with averages around 40000 and 20000, respectively, (based on data from Wasson and Kallemeyn, 1988). In comparison, Na/Sm and K/Th ratios observed in Martian meteorites are 3570–9500 and 3150–7500, respectively (Lodders, 1998), while observations from orbit suggest K/Th to be 5330 ± 220 (Taylor et al., 2007). K/Th has also been measured on Vesta (possibly EPB) by the Dawn mission, where a value of 900 ± 400 was obtained (Prettyman et al., 2015) and thus, orders of magnitudes lower compared to chondritic values. Similarly, the volatile-depleted angrites show low values for Na/Sm (39–117) and K/Th (44–875) (Warren and Kallemeyn, 1990; Mittlefehldt and Lindstrom, 1990) and may therefore be regarded as an important complement to compensate for the too high ratios that result

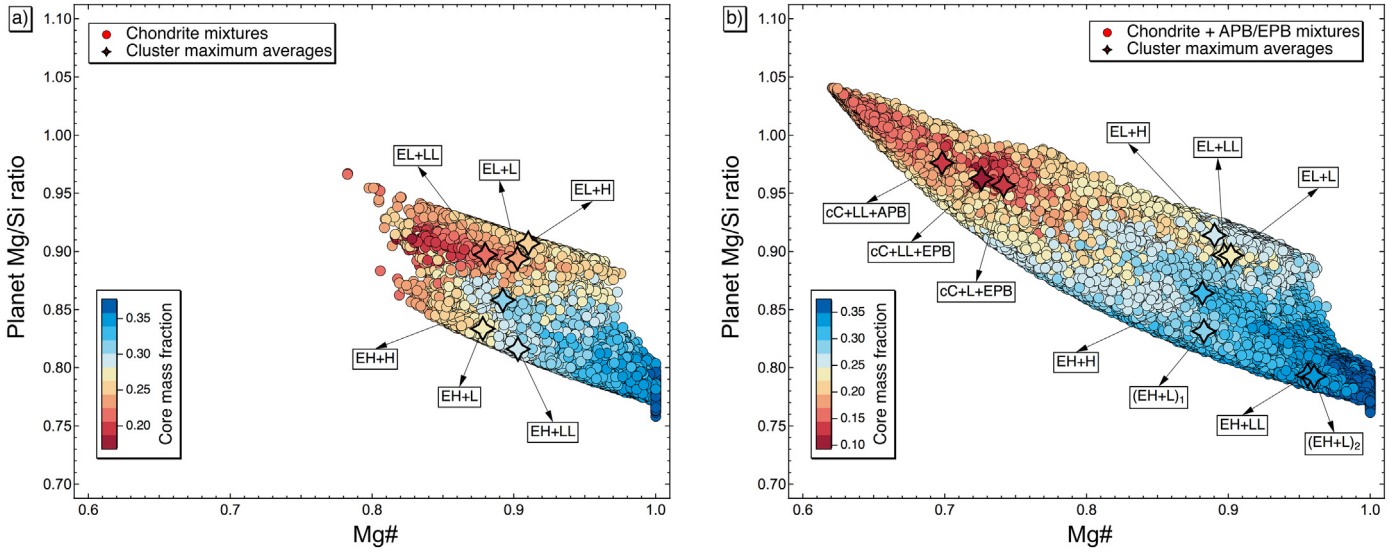

Fig. 6. Predicted bulk elemental properties (molar Mg/Si vs. Mg# (molar MgO/(MgO + FeO)) of isotopically matching mixtures for Mars if considered as a mixture of a) purely chondrites and b) chondrites and the differentiated objects: angrites (APB) and eucrites (EPB). Estimates of Mg# and Mg/Si based on several bulk compositional models of Mars (Dreibus and Wänke, 1984; Lodders and Fegley, 1997; Sanloup et al., 1999; Taylor, 2013) are ~0.75 and 0.97–1.05, respectively. Purely chondritic mixtures, if consistent with isotopic constraints of Mars, imply a significantly different bulk chemistry, whereas inclusion of APB or EPB resolves this apparent predicament.

from chondrite-only mixtures. Thus, the generally low Na/Sm or K/Th values in the differentiated objects are, next to the present geophysical considerations presented here, a further argument for their potential significance in the accretion of Mars as suggested by Fitoussi et al. (2016). However, in the absence of well-constrained bulk compositions of all meteoritic groups, any bulk Mars compositional estimate based on meteorite mixtures remains ambiguous, even if isotopically consistent.

Dynamic studies that attempt to assemble terrestrial-type planets via N-body simulations present another means for studying compositional variations in the early inner solar system (e.g., Chambers and Wetherill, 1998; Rubie et al., 2015; Brasser et al., 2017). This approach is distinct from the present study in that the compositions of the growing planets are dynamically tracked. For example, Brasser et al. (2017) considered the Grand Tack model (Walsh et al., 2011), which dynamically simulates the early gas-driven radial migration of Jupiter and Saturn, to posit that Mars must have been formed outside of the terrestrial planet feeding zone (in the general neighbourhood of the asteroid belt) on account of the observed isotopic heterogeneity and only subsequently migrated inward as a result of its gravitational interaction with Jupiter. Because of the uncertainty surrounding Mars' bulk composition, however, the compositional variety of modelled analogues of Mars was found to be large, ranging from models consisting mostly of enstatite chondrites to models made up mostly of ordinary chondrites. In addition, all the simulated bodies are incompatible with the geophysical observations.

3.2. Results for Earth

In a last step, the methodology is applied to Earth with a number of modifications. The present core model is valid for the system Fe-S (Section 2.3) and while appropriate for Mars, it is insufficient as a model of Earth's core because the latter is believed to contain up to 10 wt. % of "light elements" for which Si, O, C, S, and H are possible candidates (e.g. Poirier, 1994). Absence of a model to compute densities and melting temperatures for varying amounts of light elements, therefore calls for a different approach.

In contrast to Mars, the internal structure of Earth (e.g., core size and mass) is well known from seismology (Dziewonski and Anderson, 1981) as is the upper mantle composition from mantle-derived samples (Taylor, 1980; Lyubetskaya and Korenaga, 2007). Relying on these observations, we employ a core mass fraction of ~0.32 and an upper mantle Mg# of ~0.89 as "redox indicators" to distinguish between different isotopic matches. Fig. 7 shows the solution clusters and calculated properties (core mass fraction and Mg#) for all terrestrial matches for which 163,022 out of 10^8 mixtures were obtained. The solutions are reduced to three clusters using PCA of which two are strongly dominated by enstatite chondrites (either EH or EL). Recent models that rely on similar isotopic constraints are found within these solutions (Dauphas et al., 2014; Dauphas, 2017). The remaining "end-member" cluster on the PCA plot consists of up to ~30% of carbonaceous material (cC), ~24% APB/EPB, and for the remaining part of ordinary, mainly L, chondrites (Table 4).

In their initial redox state, only EH chondrite-rich mixtures (see cluster maxima in Fig. 7b and Table 4) are found in the immediate vicinity of the terrestrial observations. Isotopically valid solutions that are free of enstatite chondrites result in far too low core mass fractions. These redox states modelled by mass balance may be altered by reactions involving H_2O and C as discussed for Mars, in addition to SiO_2-reduction to Si metal, which provides a possible explanation for Si as a "light element" core-contaminant (Javoy, 1995, Section 2.2). The directions that mixtures may generally shift as a result of such reactions are indicated by arrows in Fig. 7b. The maximum possible changes depend on the available quantities of H_2O and C and the assumed concentration of Si in the core. The redox reaction involving carbon allows for the presence of an increasing fraction of carbonaceous material. This model presumes that Earth is accreted as an isochemical mixture of meteorites with pre-defined mantle and core components. A "moon-forming" impact, which may have disproportionately contributed to Earth's core, could significantly alter the solutions in Mg# vs core mass to larger core sizes. To strongly affect Mg#, however, would necessitate accompanying redox reactions. Thus, mixtures containing little or no material with bulk redox characteristics similar to enstatite chondrites are difficult to reconcile with the present-day Mg# of Earth's mantle.

On the other hand, Si-isotope systematics (Fitoussi and Bourdon, 2012) and major and refractory lithophile element concentrations of bulk silicate Earth are at odds with the known enstatite chondrite compositions (e.g., Fitoussi et al., 2016). Fitoussi et al. (2016) therefore argued for a mixture of 50% APB, 32% H, 10% CV, and 8% CI as a possible representation for Earth to resolve these discrepancies, which is similar to solutions found here. Mixtures in the proximity of the nearly EH- and EL-free cluster (enriched in APB), however, result by mass balance in small cores but more importantly in low Mg#'s. For the reasons discussed above, low Mg#'s are difficult to reconcile with the redox state of the upper mantle and require a mechanism for the large-scale reduction of mantle FeO. Furthermore, enstatite chondrite-poor mixtures require a homogeneous accretion scenario to match the isotopic composition of siderophile elements. For Earth, such a scenario has been questioned based on isotope systematics of highly siderophile elements (e.g. Mo, Rh), which also point towards an origin of Earth that is dominated by material that is isotopically similar to enstatite chondrites (Dauphas, 2017). To resolve the apparent discrepancy with regard to Si isotopes and bulk composition would require that Earth largely consists of material with enstatite chondrite-like isotopic signatures for most elements and a similar or slightly more oxidised redox state, but different major, minor, and trace element chemistries (Dauphas, 2017). If such a meteoritic component had become entirely consumed during accretion, it would provide an explanation for why it is not present in current meteorite collections (Drake and Righter, 2002).

3.3. Limitations of the model

In this study, we addressed a simple yet legitimate question: If chondrites are considered to be primordial planetary building blocks, are geophysical properties of the terrestrial planets consistent with isochemical mixtures of these? The present analysis has shown how predicted geophysical properties of isotopically valid meteoritic mixtures can be employed to further discriminate between various solutions. The general methodology relies on mass balance, which is robust, but bound to certain limitations that will be discussed in the following.

Estimating the maximum possible changes in core size and mantle FeO concentration for the different meteoritic mixtures is based on reactions involving the redox partners H_2O and C, whose abundances are calculated from meteorite averages. Although such averages may have been influenced by processes on their parent bodies (e.g. Grimm and McSween., 1989), they provide a reasonable estimate to gauge the magnitude of possible core-mantle redox exchange. Significant additional accretion of H_2O via sources other than considered here, would call for special consideration in terms of isotopic (i.e., $\Delta'^{17}O$) and potential redox effects. Note that any late addition of water after core formation has ceased entirely, may change the ferric/ferrous ratio of the silicate but is unlikely to alter core size significantly.

As a final comment, we would like to emphasise that the bulk redox state of a planet is determined by oxidation state, chemical composition, and order of addition of accreted material, unless the bulk core-silicate ratio is altered by collisional erosion. Mass exchange between core and mantle, i.e., element partitioning between these reservoirs, is bound to redox reactions for most elements, which requires the presence of appropriate redox partners in the accreted material. For Mars, we showed that oxidised material in addition to that provided by chondritic mixtures is required. In contrast, Mercury, with a core mass

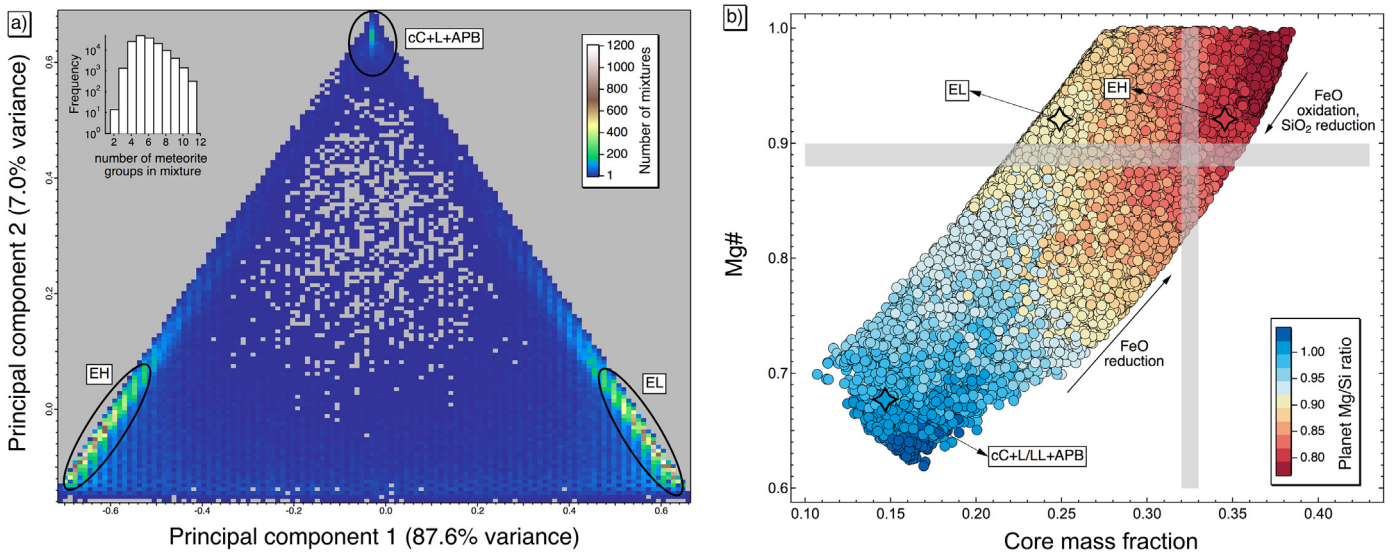

Fig. 7. Mixing solutions for Earth based on chondrite and achondrite (differentiated objects) material. a) Principal component analysis showing the first two principal components, which account for > 95% of the variance. Compared to Mars (Fig. 5) there are only three solution clusters (outlined in black), of which two are dominated by enstatite chondrites (EH and EL). A third cluster contains a maximum of 38% carbonaceous chondrites with, on average, about one third L and LL and differentiated meteorites such as angrites (APB). The inset (histogram) shows the distribution in number of meteorites that contribute to all matching solutions. b) Major element composition of matching solutions, including cluster averages, in terms of Mg# and Mg/Si versus core mass fraction. Grey bars indicate ranges for the upper mantle Mg# and Earth's core mass fraction. Each data point is representative of the initial redox state of the mixtures. The diagonal arrows indicate the general direction in which redox reactions may shift the distribution (see text for details).

fraction of ~0.8 (e.g., Hauck et al., 2013; Padovan et al., 2014), has a significantly higher metal-to-silicate ratio than can be imposed by enstatite chondrites (~0.4, Table 1). This suggests that components with possibly higher metal/silicate ratios are involved in Mercury's accretion, or that parts of the mantle were removed through impacts (e.g., Benz et al., 1988). Irrespectively, it is our contention that considering geophysical properties and redox ranges of isochemical mixtures of planetary building blocks provides important insights on planetary accretion in the Solar System.

4. Conclusions

This contribution has shown that consideration of isotope data alone is insufficient as a means of distinguishing between terrestrial planet building blocks. Instead, geochemical, geophysical, and bulk elemental considerations should be considered in an integrated manner to advance our understanding of the nature of the material from which the terrestrial planets are made. More specifically, we showed that

- Isotopically matching chondritic mixtures for Mars result in compositions that are too reduced to be consistent with current Martian geophysical observations.
- Instead, Mars is found to partly consist of a relatively oxidised component, such as the angrite parent body. Because of the uncertainty on the bulk composition of such an object, an inherent ambiguity surrounds the exact mixing proportions of the various chondritic and achondritic components and, as a result, Mars' bulk chemical composition.
- To produce less ambiguous bulk compositional estimates of the terrestrial planets based on meteoritic mixing models, better compositional constraints on differentiated objects are needed.
- The question of what the Earth is made of remains elusive. Based on the redox analysis conducted here, Earth appears to have accreted a large proportion of enstatite chondrite-like material.

Finally, we expect that the Mars InSight mission (Banerdt et al., 2013), which has landed a geophysical package including a seismometer, heat flow probe, magnetometer, and geodetic instrument on the surface of Mars, will enable stronger constraints to be placed on its interior and possibly its building blocks.

Acknowledgements

The authors would like to thank J.A.D. Connolly, M. Schönbächler, A. Trinquier and M. Rüfenacht for helpful discussions. The manuscript benefited from reviews by Nicolas Dauphas, Caroline Fitoussi, and an anonymous reviewer. A.K. and C.L. would like to acknowledge the support from the Swiss National Science Foundation (SNF project 172508 “Mapping the internal structure of Mars”) and ETH Zürich (ETH-1017-1), respectively.

Appendix A

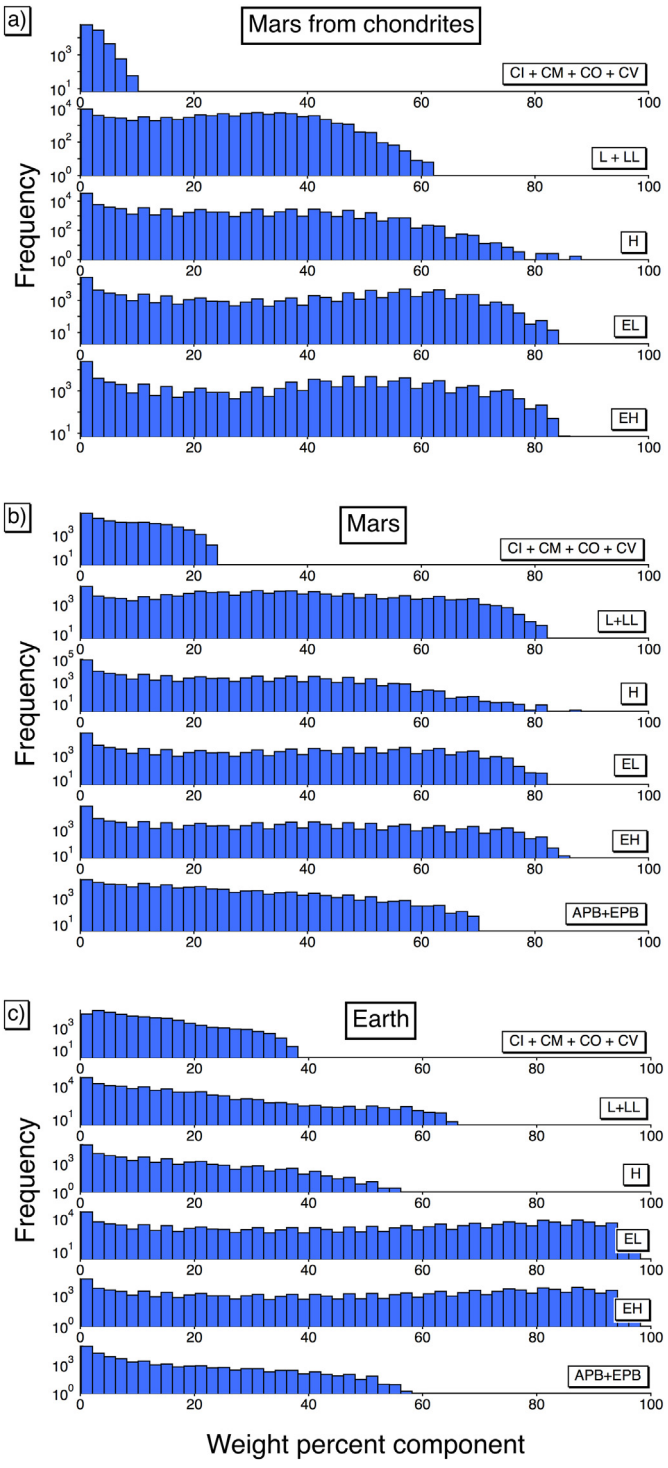

Fig. A.8. Log-based histograms showing weight fractions of different meteoritic groups for all isotopically matching mixtures. a) Solutions for Mars with chondritic mixtures only; b)—c) are for mixtures including differentiated achondrites (angrites and eucrites) that reproduce Mars and Earth, respectively.

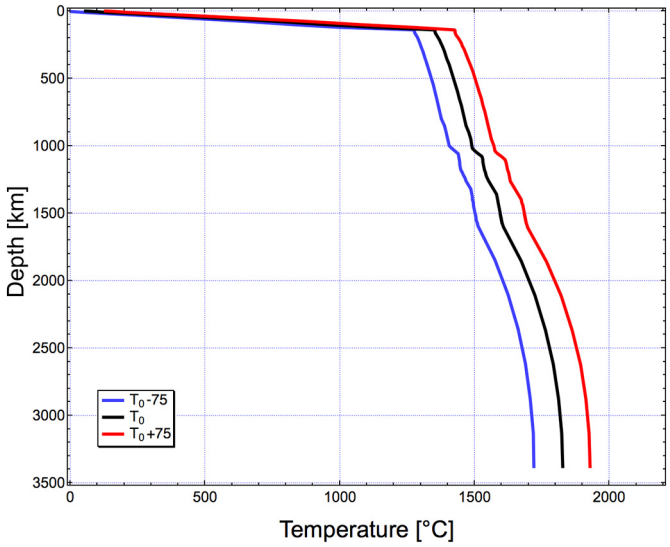

Fig. A.9. Martian model areotherms. The model areotherms are assumed conductive in the crust and lithosphere and adiabatic beneath. Mantle adiabats are computed self-consistently using thermodynamic principles as described in Section 2.3. T_0 refers to a reference geothermal profile used in all calculations.

References

Agee, C.B., Draper, D.S., 2004. Experimental constraints on the origin of Martian meteorites and the composition of the Martian mantle. Earth Planet. Sci. Lett. 224, 415–429.

Allègre, C., Manhès, G., Lewin, É., 2001. Chemical composition of the Earth and the volatility control on planetary genetics. Earth Planet. Sci. Lett. 185, 49–69.

Anders, E., Grevesse, N., 1989. Abundances of the elements - meteoritic and solar. Geochim. Cosmochim. Acta 53 (1), 197–214.

Ashcroft, H., Wood, B., 2015. An experimental study of partial melting and fractional crystallization on the HED parent body. Meteorit. Planet. Sci. 50 (11), 1912–1924.

Banerdt, W.B., Smrekar, S., Lognonné, P., Spohn, T., Asmar, S.W., Banfield, D., Boschi, L., Christensen, U., Dehant, V., Folkner, W., Giardini, D., Goetze, W., Golombek, M., Grott, M., Hudson, T., Johnson, C., Kargl, G., Kobayashi, N., Maki, J., Mimoun, D., Mocquet, A., Morgan, P., Panning, M., Pike, W.T., Tromp, J., van Zoest, T., Weber, R., Wieczorek, M.A., Garcia, R., Hurst, K., 2013. InSight: A Discovery mission to explore the interior of Mars. In: Lunar and Planetary Science Conference. Lunar and Planetary Inst. Technical Report. vol. 44. pp. 1915 Mar.

Benz, W., Slattery, W.L., Cameron, A.G.W., 1988. Collisional stripping of Mercury's mantle. Icarus 74, 516–528 Jun.

Bonnand, P., Williams, H.M., Parkinson, I.J., Wood, B.J., Halliday, A.N., 2016. Stable chromium isotopic composition of meteorites and metal-silicate experiments: implications for fractionation during core formation. Earth Planet. Sci. Lett. 435, 14–21.

Borg, L.E., Draper, D.S., 2003. A petrogenic model for the origin and compositional variation of the Martian basaltic meteorites. Meteorit. Planet. Sci. 38, 1713–1731.

Brasser, R., Mojzsis, S., Matsumura, S., Ida, S., 2017. The cool and distant formation of Mars. Earth Planet. Sci. Lett. 468, 85–93.

Burbine, T.H., O'Brien, K.M., 2004. Determining the possible building blocks of the Earth and Mars. Meteorit. Planet. Sci. 39, 667–681.

Burkhardt, C., Dauphas, N., Tang, H., Fischer-Goedde, M., Qin, L., Chen, J.H., Rout, S.S., Pack, A., Heck, P.R., Papanastassiou, D.A., 2017. In search of the Earth-forming reservoir: mineralogical, chemical, and isotopic characterizations of the ungrouped achondrite NWA 5363/NWA 5400 and selected chondrites. Meteorit. Planet. Sci. 52 (5), 807–826.

Chambers, J., Wetherill, G., 1998. Making the terrestrial planets: N-body integrations of planetary embryos in three dimensions. Icarus 136 (2), 304–327.

Connolly, J.A.D., 2009. The geodynamic equation of state: what and how. Geochem. Geophys. Geosyst. 10 (10), Q10014.

Cook, D.L., Wadhwa, M., Clayton, R.N., Dauphas, N., Janney, P.E., Davis, A.M., 2007. Mass-dependent fractionation of nickel isotopes in meteoritic metal. Meteorit. Planet. Sci. 42 (12), 2067–2077.

Dauphas, N., 2017. The isotopic nature of the Earth's accreting material through time. Nature 541 (7638), 521–524.

Dauphas, N., Chen, J.H., Zhang, J., Papanastassiou, D.A., Davis, A.M., Travaglio, C., 2014. Calcium-48 isotopic anomalies in bulk chondrites and achondrites: evidence for a uniform isotopic reservoir in the inner protoplanetary disk. Earth Planet. Sci. Lett. 407, 96–108.

Drake, M., Righter, K., 2002. Determining the composition of the earth. Nature 416 (6876), 39–44.

Dreibus, G., Wänke, H., 1984. Accretion of the earth and inner planets. In: Geochemistry and Cosmochemistry, pp. 3–11.

Dreibus, G., Wänke, H., 1985. Mars, a volatile-rich planet. Meteoritics 20, 367–381.

Dziewonski, A.M., Anderson, D.L., 1981. Preliminary reference Earth model. Phys. Earth Planet. Inter. 25, 297–356.

Esposito, P.B., Banerdt, W.B., Lindal, G.F., Sjogren, W.L., Slade, M.A., Bills, B.G., Smith, D.E., Balmino, G., 1992. Gravity and Topography. pp. 209–248.

Fitoussi, C., Bourdon, B., 2012. Silicon isotope evidence against an enstatite chondrite Earth. Science 335 (6075), 1477–1480.

Fitoussi, C., Bourdon, B., Wang, X., 2016. The building blocks of Earth and Mars: a close genetic link. Earth Planet. Sci. Lett. 434, 151–160.

Genova, A., Goossens, S., Lemoine, F.G., Mazarico, E., Neumann, G.A., Smith, D.E., Zuber, M.T., 2016. Seasonal and static gravity field of Mars from MGS, Mars Odyssey and MRO radio science. Icarus 272, 228–245.

Grimm, R., McSween, H., 1989. Water and the thermal evolution of carbonaceous chondrite parent bodies. Icarus 82 (2), 244–280.

Hauck, S.A., Margot, J.-L., Solomon, S.C., Phillips, R.J., Johnson, C.L., Lemoine, F.G., Mazarico, E., McCoy, T.J., Padovan, S., Peale, S.J., Perry, M.E., Smith, D.E., Zuber, M.T., 2013. The curious case of mercury's internal structure. J. Geophys. Res. Planets 118 (6), 1204–1220.

Jarosewich, E., 1990. Chemical analysis of meteorites - a compilation of stony and iron meteorite analyses. Meteoritics 25 (4), 323–337.

Javoy, M., 1995. The integral enstatite chondrite model of the Earth. Geophys. Res. Lett. 22 (16), 2219–2222.

Javoy, M., Kaminski, E., Guyot, F., Andrault, D., Sanloup, C., Moreira, M., Labrosse, S., Jambon, A., Agrinier, P., Davaille, A., Jaupart, C., 2010. The chemical composition of the Earth: enstatite chondrite models. Earth Planet. Sci. Lett. 293 (3-4), 259–268.

Jurewicz, A., Mittlefehldt, D., Jones, J., 1991. Partial melting of the Allende (CV3) meteorite - implications for origins of basaltic meterorites. Science 252 (5006), 695–698.

Jurewicz, A., Mittlefehldt, D., Jones, J., 1993. Experimental partial melting of the Allende (CV3) and Murchison (CM) chondrites and the origin of asteroidal basalts. Geochim. Cosmochim. Acta 57 (9), 2123–2139.

Khan, A., Liebske, C., Rozel, A., Rivoldini, A., Nimmo, F., Connolly, J.A.D., Plesa, A.-C., Giardini, D., 2018. A geophysical perspective on the bulk composition of Mars. J. Geophys. Res. Planets 123, 575–611. https://doi.org/10.1002/2017JE005371.

Konopliv, A.S., Park, R.S., Folkner, W.M., 2016. An improved JPL Mars gravity field and orientation from Mars orbiter and lander tracking data. Icarus 274, 253–260.

Liebske, C., 2015. iSpectra: an open source toolbox for the analysis of spectral images recorded on scanning electron microscopes. Microsc. Microanal. 21 (4), 1006–1016.

Lodders, K., 1998. A survey of shergottite, nakhlite and chassigny meteorites whole-rock compositions. Meteorit. Planet. Sci. 33 (4 Suppl.), A183–A190.

Lodders, K., 2000. An oxygen isotope mixing model for the accretion and composition of rocky planets. Space Sci. Rev. 92, 341–354.

Lodders, K., Fegley, B., 1997. An oxygen isotope model for the composition of Mars. Icarus 126 (2), 373–394.

Lyubetskaya, T., Korenaga, J., 2007. Chemical composition of earth's primitive mantle and its variance: 1. method and results. J. Geophys. Res. Solid Earth 112 (B3) B03211.

Mann, U., Frost, D.J., Rubie, D.C., 2009. Evidence for high-pressure core-mantle differentiation from the metal-silicate partitioning of lithophile and weakly-siderophile elements. Geochim. Cosmochim. Acta 73 (24), 7360–7386.

McSween Jr., H.Y., McLennan, S.M., 2014. Mars. In: Turekian, K., Holland, H. (Eds.), Planets, Asteriods, Comets and The Solar System. Elsevier Science, pp. 251–300.

Mittlefehldt, D., Lindstrom, M., 1990. Geochemistry and genesis of the angrites. Geochim. Cosmochim. Acta 54 (11), 3209–3218.

Mohapatra, R.K., Murty, S.V.S., 2003. Precursors of Mars-constraints from nitrogen and oxygen isotopic compositions of martian meteorites. Meteorit. Planet. Sci. 38,

225–242.
Mosegaard, K., Tarantola, A., 1995. Monte Carlo sampling of solutions to inverse problems. J. Geophys. Res. Solid Earth (1978–2012) 100 (B7), 12431–12447.
Mougel, B., Moynier, F., Göpel, C., 2018. Chromium isotopic homogeneity between the moon, the earth, and enstatite chondrites. Earth Planet. Sci. Lett. 481, 1–8.
Padovan, S., Margot, J.-L., Hauck, S.A., Moore, W.B., Solomon, S.C., 2014. The tides of mercury and possible implications for its interior structure. J. Geophys. Res. Planets 119 (4), 850–866.
Palme, H., O'Neill, H.S.C., 2003. Cosmochemical estimates of mantle composition. Treatise Geochem. 2, 568.
Poirier, J.-P., 1994. Light elements in the Earth's outer core: a critical review. Phys. Earth Planet. Inter. 85, 319–337. https://doi.org/10.1016/0031-9201(94)90120-1.
Prettyman, T., Yamashita, N., Reedy, R., McSween Jr., H.Y., Mittlefehldt, D., Hendricks, J., Toplis, M., 2015. Concentrations of potassium and thorium within vesta's regolith. Icarus 259, 39–52.
Qin, L., Carlson, R.W., 2016. Nucleosynthetic isotope anomalies and their cosmochemical significance. Geochem. J. 50 (1, SI), 43–65.
Righter, K., Drake, M.J., Scott, E.R.D., 2006. Compositional Relationships Between Meteorites and Terrestrial Planets. pp. 803–828.
Rivoldini, A., Van Hoolst, T., Verhoeven, O., Mocquet, A., Dehant, V., 2011. Geodesy constraints on the interior structure and composition of Mars. Icarus 213, 451–472.
Roberts, J.H., Nimmo, F., 2008. Tidal heating and the long-term stability of a subsurface ocean on Enceladus. Icarus 194, 675–689 Apr.
Rubie, D., Jacobson, S., Morbidelli, A., O'Brien, D., Young, E., de Vries, J., Nimmo, F., Palme, H., Frost, D., 2015. Accretion and differentiation of the terrestrial planets with implications for the compositions of early-formed solar system bodies and accretion of water. Icarus 248, 89–108.
Russell, C.T., Raymond, C.A., Coradini, A., McSween, H.Y., Zuber, M.T., Nathues, A., De Sanctis, M.C., Jaumann, R., Konopliv, A.S., Preusker, F., Asmar, S.W., Park, R.S., Gaskell, R., Keller, H.U., Mottola, S., Roatsch, T., Scully, J.E.C., Smith, D.E., Tricarico, P., Toplis, M.J., Christensen, U.R., Feldman, W.C., Lawrence, D.J., McCoy, T.J., Prettyman, T.H., Reedy, R.C., Sykes, M.E., Titus, T.N., 2012. Dawn at Vesta: Testing the Protoplanetary Paradigm. Science 336 (6082), 684–686.
Sanloup, C., Jambon, A., Gillet, P., 1999. A simple chondritic model of Mars. Phys. Earth Planet. Inter. 112 (1–2), 43–54.
Schönbächler, M., Rehkamper, M., Fehr, M., Halliday, A., Hattendorf, B., Günther, D., 2005. Nucleosynthetic zirconium isotope anomalies in acid leachates of carbonaceous chondrites. Geochim. Cosmochim. Acta 69 (21), 5113–5122.
Seidelmann, P.K., Abalakin, V.K., Bursa, M., Davies, M.E., de Bergh, C., Lieske, J.H., Oberst, J., Simon, J.L., Standish, E.M., Stooke, P., Thomas, P.C., 2002. Report of the IAU/IAG Working Group on cartographic coordinates and rotational elements of the planets and satellites: 2000. Celest. Mech. Dyn. Astron. 82 (1), 83–111.
Steenstra, E.S., Sitabi, A.B., Lin, Y.H., Rai, N., Knibbe, J.S., Berndt, J., Matveev, S., van Westrenen, W., 2017. The effect of melt composition on metal-silicate partitioning of siderophile elements and constraints on core formation in the angrite parent body. Geochim. Cosmochim. Acta 212, 62–83.
Stewart, A.J., Schmidt, M.W., van Westrenen, W., Liebske, C., 2007. Mars: a new core-crystallization regime. Science 316, 1323.
Stixrude, L., Lithgow-Bertelloni, C., 2005. Mineralogy and elasticity of the oceanic upper mantle: origin of the low-velocity zone. J. Geophys. Res. Solid Earth 110 (B3). https://doi.org/10.1029/2004JB002965. B03204.
Stixrude, L., Lithgow-Bertelloni, C., 2011. Thermodynamics of mantle minerals - II. Phase equilibria. Geophys. J. Int. 184, 1180–1213 Mar.
Tang, H., Dauphas, N., 2014. Fe-60-Ni-60 chronology of core formation in Mars. Earth Planet. Sci. Lett. 390, 264–274.
Taylor, G., Stopar, J., Boynton, W., Karunatillake, S., Keller, J., Brückner, J., Wänke, H., Dreibus, G., Kerry, K., Reedy, R., Evans, L., Starr, R., Martel, L., Squyres, S., Gasnault, O., Maurice, S., d'Uston, C., Englert, P., Dohm, J., Baker, V., Hamara, D., Janes, D., Sprague, A., Kim, K., Drake, D., McLennan, S., Hahn, B., 2007. Variations in k/th on Mars. J. Geophys. Res. E Planets 112 (3).
Taylor, G.J., 2013. The bulk composition of Mars. Chem. Erde / Geochem. 73, 401–420 Dec.
Taylor, S.R., 1980. Refractory and moderately volatile element abundances in the earth, moon and meteorites. In: Bedini, S.A. (Ed.), Lunar and Planetary Science Conference Proceedings. Lunar and Planetary Science Conference Proceedings. vol. 11. pp. 333–348.
Taylor, S.R., 2001. Solar System Evolution: A New Perspective. Cambridge University Press.
Taylor, S.R., McLennan, S., 2009. Planetary Crusts: Their Composition, Origin and Evolution. Blackwell Publishing Ltd.
Trinquier, A., Birck, J.-L., Allegre, C.J., 2007. Widespread cr-54 heterogeneity in the inner solar system. Astrophys. J. 655 (2, 1), 1179–1185.
Wadhwa, M., 2001. Redox state of Mars' upper mantle and crust from Eu anomalies in shergottite pyroxenes. Science 291, 1527–1530.
Walsh, K.J., Morbidelli, A., Raymond, S.N., O'Brien, D.P., Mandell, A.M., 2011. A low mass for Mars from Jupiter's early gas-driven migration. Nature 475, 206–209.
Warren, P., Kallemeyn, G., 1990. Geochemistry of the LEW87051 angrite, and other basaltic achondrites. Lunar Planet. Sci. Conf. (21), 1295–1296.
Warren, P.H., 2011. Stable-isotopic anomalies and the accretionary assemblage of the Earth and Mars: a subordinate role for carbonaceous chondrites. Earth Planet. Sci. Lett. 311 (1–2), 93–100.
Wasson, J.T., Kallemeyn, G.W., 1988. Compositions of chondrites. Philos. Trans. R. Soc. Lond. A 325, 535–544.
Yoder, C.F., Konopliv, A.S., Yuan, D.N., Standish, E.M., Folkner, W.M., 2003. Fluid core size of Mars from detection of the solar tide. Science 300, 299–303.